Mamman *et al.*
Journal of Analytical Science and Technology (2023) 14:3
https://doi.org/10.1186/s40543-023-00367-4

Journal of Analytical Science and Technology

RESEARCH ARTICLE

Open Access

Exploring the performance of magnetic methacrylic acid-functionalized β-cyclodextrin adsorbent toward selected phenolic compounds

S. Mamman[1,2,4], S. F. F. S. Yaacob[1], M. Raoov[3], F. S. Mehamod[5], N. N. M. Zain[2*] and F. B. M. Suah[1*]

Abstract

In this study, the removal of bisphenol A (BPA), 2,4-dinitrophenol (2,4-DNP), and 2,4-dichlorophenol (2,4-DCP) using a new magnetic adsorbent methacrylic acid-functionalized β-cyclodextrin (Fe_3O_4@MAA-βCD) was evaluated. The materials were characterized by Fourier transform infrared spectroscopy, scanning electron microscope, transmission electron microscopy, and X-ray diffraction. The batch adsorption experiments optimized and evaluated various operational parameters such as pH, contact time, sorbent dosage, initial concentration, and temperature. The result shows that DNP possessed the most excellent affinity toward Fe_3O_4@MAA-βCD adsorbents compared to BPA and DCP. Also, BPA showed the lowest removal and was used as a model analyte for further study. The adsorption kinetic data revealed that the uptake of these compounds follows the pseudo-second order. Freundlich and Halsey isotherms best-fitted the adsorption equilibrium data. The desorption process was exothermic and spontaneous, and a lower temperature favored the adsorption. Furthermore, hydrogen bonding, inclusion complexion, and π–π interactions contributed to the selected phenolic compound's adsorption.

Keywords Adsorption, Magnetic nanoparticles, Phenolic compounds, β-cyclodextrin

Introduction

Phenol and its analogs are highly poisonous and can be absorbed into the human body (Dada et al. 2017). Because of the dangers posed by their presence, regulatory bodies like the United States Environmental Protection Agency (USEPA) (Bohdziewicz et al. 2012), the European Union (EU) (Hairuddin et al. 2019), and the World Health Organization (WHO) have listed them in their respective priority pollutant lists. It has been determined that the acceptable level of phenolic compounds in wastewater is 1 ppm, while the acceptable level in potable water is less than 0.001 ppm (Sas et al. 2019).

In the past few years, adsorption has demonstrated promising and effective outcomes as a treatment technology for wastewater produced on a laboratory scale. As a result, various adsorbents for removing phenolic substances from wastewater samples have been synthesized

*Correspondence:
N. N. M. Zain
nurnadhirah@usm.my
F. B. M. Suah
fsuah@usm.my
[1] School of Chemical Sciences, Universiti Sains Malaysia, 11800 George Town, Pulau Pinang, Malaysia
[2] Integrative Medicine Cluster, Advanced Medical and Dental Institute, Universiti Sains Malaysia, 13200 Kepala Batas, Penang, Malaysia
[3] Department of Chemistry, Faculty of Science, Universiti Malaya, 50603 Kuala Lumpur, Malaysia
[4] Faculty of Natural and Applied Sciences Department of Chemistry, Nasarawa State University Keffi, PMB 1022, Keffi, Nasarawa State, Nigeria
[5] Advanced Nano Materials (ANoMA) Research Group, School of Fundamental Science, Universiti Malaysia Terengganu, 21030 Kuala Nerus, Terengganu, Malaysia

and employed based on the reported literature (Sas et al. 2020; Abdel-Ghani et al. 2016; Abdoli et al. 2015; Allaboun and Abu Al-Rub 2016; Balci and Erkurt 2017; Biglari et al. 2017; Magdy et al. 2018; Mohamed et al. 2011). However, before adsorption can be completely implemented by industries, several hurdles must be overcome, including high capital costs, challenging adsorbent separation from solution samples, and a complicated manufacturing process.

The use of magnetism in an adsorption process is a relatively newer concept, gathering increasing attention from researchers from multiple fields because of their unusual magnetic characteristics (Magdy et al. 2018; Mohamed et al. 2011; Tursi et al. 2018; Zain et al. 2016). Iron oxide nanoparticles are widely studied due to their high adsorption capacity of pollutants, magnetic properties, and biocompatibility (Santhosh et al. 2017). Despite these, the unavoidable problem of unmodified iron oxide nanoparticles, such as agglomeration, would cause a limit on their application (Sas et al. 2019; Ismail et al. 2013; Spiridon et al. 2015). Thus, it is necessary to develop strategies to overcome the problem of unmodified ferromagnetic nanoparticles by considering a good way to functionalize nanoparticles (Jain et al. 2018).

Over the past decades, synthetic polymer adsorbents have emerged as an efficient adsorbent that effectively traps many pervasive organic pollutants in an aqueous solution because of their excellent mechanical strength, elastic surface chemistry, and pore size distribution. Also, the feasibility of regeneration in moderate conditions and the potential removal of some organic compounds make this technology outstanding (Xiao et al. 2012). Moreover, the magnetic polymeric adsorbent is an inexpensive alternative to extensively activated charcoal for organic pollutant removal (Xiao et al. 2012). Many polymer adsorbents achieve stronger adsorption and selectivity for some persistent pollutants through chemical modification by cross-linking/grafting certain unique functional groups (Spiridon et al. 2015; Jain et al. 2018; Xiao et al. 2012; Raoov et al. 2013; Yang et al. 2016; Rashid et al. 1123; Surikumaran et al. 2014, 2015; Asiri et al. 2015). β-cyclodextrin (β-CD) is a renewable and biodegradable compound, consisting of a cyclic oligosaccharide containing 7 glucopyranoside units which are bounded by α (1–4), which produces a torus-shaped structure, with an internal hydrophobic and an external hydrophilic cavity which forms inclusion complex with various molecules by incorporating them into the cavity (Surikumaran et al. 2015; Anne et al. 2018). Due to its unique properties, β-CD has attracted the interest of multiple researchers (Xiao et al. 2012; Raoov et al. 2013; Yang et al. 2016; Rashid et al. 1123; Surikumaran et al. 2014, 2015; Asiri et al. 2015; Anne et al. 2018; Guo et al. 2013; Mohammadzadeh Kakhki 2015; Moulahcene et al. 2016; Li et al. 2012; Folch-Cano et al. 2014; Han et al. 2015). Some studies have shown that β-CD can also increase magnetic nanoparticles' stability in water, thus strengthening their dispersal over a long time in the aqueous medium. Some studies have shown that β-CD can also increase magnetic nanoparticles' strength in water, thus maintaining their dispersion over a long time in the aqueous medium (Monteiro et al. 2017).

In this study, we synthesized Fe_3O_4@MAA-βCD composite via a one-step co-precipitation method. The investigation devoted to studying and evaluating the effectiveness of the newly synthesized Fe_3O_4@MAA-βCD as an adsorbent for the removal of bisphenol A (BPA), 2,4-dinitrophenol (2,4-DNP), and 2,4-dichlorophenol (2,4-DCP) from real environmental water samples. The magnetic properties of Fe_3O_4 provide large surface area; paramagnetic properties for ease separation, stability, less toxicity, ease of synthesis as well as versatile functionalization deserve particular consideration. The role of host guest encapsulation of β-cyclodextrin makes it a suitable host candidate to entrap and remove the phenolic compound from environmental samples by applying the adsorption technique. In addition, the hydrogen bonding and π–π interaction that could be formed with phenolic compound would allow the modified nanocomposite to selectively entrap and bind the phenolic compounds at the surface.

Experimental

Materials and reagents

Methacrylic acid (MAA), toluene 2,4-diisocyanate (TDI), dimethylacetamide (DMAC), BPA, 2,4-DCP, 2,4-DNP, β-CD, and dibutyltin dilaurate (DBTDL) were procured from Sigma-Aldrich (USA). Iron (II) chloride tetrahydrate ($FeCl_2{\cdot}4H_2O$) and iron (III) chloride hexahydrate ($FeCl_3{\cdot}6H_2O$) were purchased from R&M (Essex, UK). Analytical grade absolute ethanol (denatured, 99.7) and methanol were acquired from HmbG Chemicals (Cologne, Germany); ammonia solution (28%) and acetic acid were purchased from Bright Chem Sdn. Bhd. Nitrogen gas was obtained from Malaysian oxygen (MOx). The stock solution of 1000 mg/L BPA DCP and DNP was prepared by diluting respective standards in methanol and stored at 4 °C. New working standards were prepared daily by diluting stock solution in deionized water. All reagents and chemicals were of analytical reagent grade and were used as received without further purification.

Instrumentation

After the adsorption experiment, UV–Vis spectrophotometer (PerkinElmer Lambda 35) was used to monitor the residual concentrations of BPA, DNP, and DCP

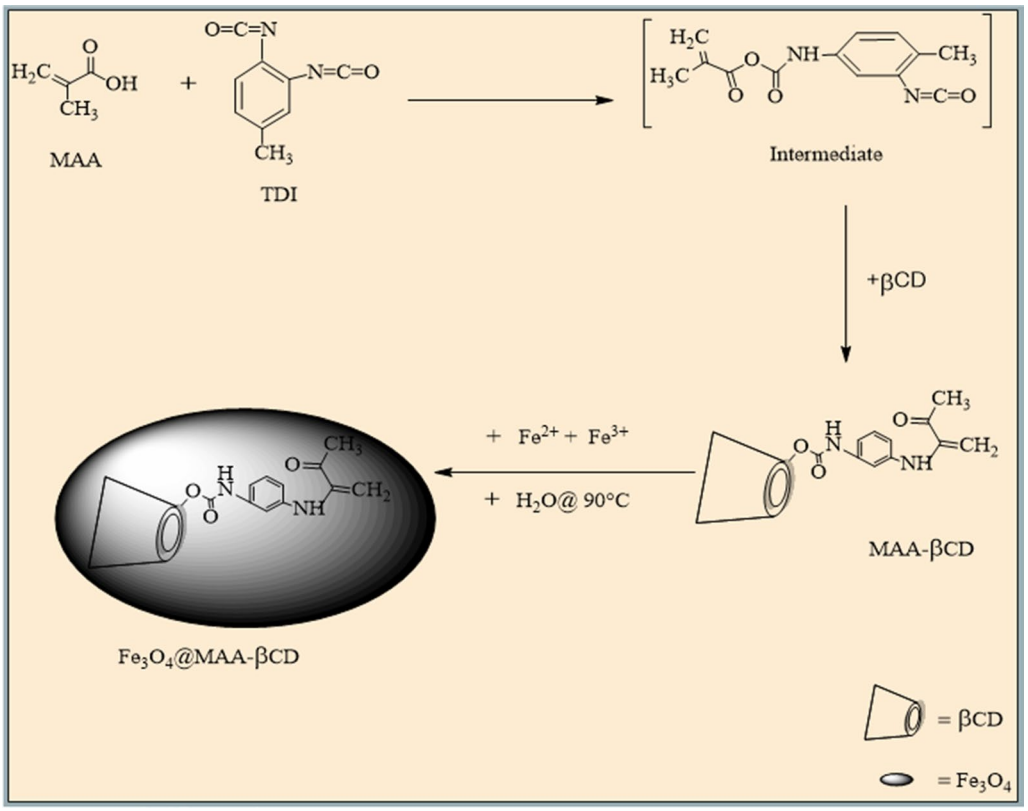

Scheme 1 Synthetic pathway for Fe_3O_4@ MAA-βCD

at λ_{max} of 276, 358, and 286 nm, respectively. Deionized water was obtained from Sartorius Stedim deionized water dispenser, Milli-Q system (Arium 611 DI). A pH meter (Eutech pH 700) was used to measure pH values. Using different temperatures, the incubator (IKA, KS4000-I control) agitates the adsorbent–adsorbate mixture at 250 rpm. An external magnet was used to separate the adsorbent from the aqueous phase.

Synthesis of adsorbent

The stoichiometric ratio was selected as 0.5 MAA: 1 M TDI: 0.5 M β-CD. To react one –OH group of β-CD, first, MAA and TDI were mixed with the DMAC solvent. After that, the solution was magnetically stirred for 1 h in nitrogen gas, and 0.1% of DBTDL catalyst was added. A few drops of this (MAA-TDI) solution were subjected to FTIR analysis. A calculated amount of β-CD and another 10 mL of DMAC were introduced into the reaction mixture and stirred for 2 h. The finished product (MAA-βCD) was obtained. Additionally, Fe_3O_4@MAA-βCD was prepared via a one-step co-precipitation method under nitrogen. MAA-βCD, $FeCl_2{\cdot}4H_2O$, and $FeCl_3{\cdot}6H_2O$ in the ratio 1:2:3 were weighed into a flask, and 100 mL of deionized water was added and stirred for 30 min at 1200 rpm under a nitrogen atmosphere. About 12 mL of NH_3 solution was added, the temperature was raised to 90 °C, and the reaction mixture was stirred for 1 h. The resultant black precipitated product was separated by an external magnetic field and dried in an oven overnight. Scheme 1 shows the synthetic pathway of Fe_3O_4@ MAA-βCD.

Characterization techniques

The adsorbent was characterized using Fourier transform infrared spectroscopy (FTIR), scanning electron microscope (SEM), vibrating sample magnetometer (VSM), X-ray diffraction (XRD), and transmission electron microscopy (TEM) to investigate Fe_3O_4@MAA-βCD composition, surface, and magnetic strength. A PerkinElmer FTIR spectrometer was used at 4000–400 cm^{-1} with 32 scans. The adsorbents were pressed into a thin disk using potassium bromide (KBr) powder under a high-pressure hydraulic press. The sample's surface morphology was examined using a QUANTA FEG450 scanning electron microscope (SEM; Czech Republic). Magnetization measurements were performed on Lakeshore 7404 series vibrating sample magnetometer (VSM; McCorkle Boulevard, Westerville, Ohio, USA).

The Philips CM12 Version Transmission electron microscope was used to determine the size and morphology of the particles, while the XRD analysis was executed using a PANalytical Empyrean model. The sample analysis was performed under Cu Kα radiation ($\lambda = 1.5418\ \Delta$).

Batch adsorption experiment

A batch adsorption study investigated the effects of experimental parameters such as pH, contact time, adsorbent dose, initial concentration and temperature, and reusability on the absorptive removal of phenolic compounds. A 20 mg of Fe_3O_4@MAA-βCD was weighed, and 10 mL of 10 mg/L adsorbate solution was added into a glass vial and sealed firmly. The vial content was agitated for 60 min at 250 rpm and 298 K using a shaker. After the adsorption, the adsorbent was separated from the supernatant using an external magnetic field. The solution was filtered and analyzed using the UV–Vis spectrometer at 276, 358, and 286 nm for BPA, DNP, and DCP, respectively. The removal efficiency was calculated using Eq. (1):

$$\text{Removal percentage}(\%) = \frac{(C_o - C_f)}{C_o} \times 100 \qquad (1)$$

where C_o and C_f is the initial concentration and final concentration, respectively (mg L^{-1}).

The uptake of the selected phenolic compounds at equilibrium is defined as the adsorption capacity, q_e (mg g^{-1}), calculated using Eq. (2):

$$q_e = \frac{[(C_o - C_f) \times V]}{w} \qquad (2)$$

where q_e is the adsorption capacity (mg g^{-1}), V (L) is the volume of the analyte, and w (g) is the mass of the adsorbent used.

Real sample analysis

Four environmental water samples were collected and analyzed to confirm the validity of the application for the proposed method. The samples were filtered through a 0.45-µm filter before being used and analyzed. Spiked samples at three different concentrations have been applied to the proposed method's removal study to check its accuracy.

The reproducibility and repeatability study of the proposed method was presented as inter-day and intraday analysis. Low, medium, and high concentrations (1, 10, and 60 mg L^{-1}) were used. The intraday triplicate determination for each vial, at each concentration level, was conducted in five separate vials ($n = 5$) within the same day. Thus, similar procedures were followed for inter-day for 5 successive days ($n = 5$) to obtain the percentage removal and relative standard deviation (%) values. The removal was carried out in triplicates ($n = 3$) for each of the concentrations tested. The percentage of removal was computed using Eq. (1).

For the reusability process, an ultrasonically methanol wash was conducted after the adsorption experiment to remove the adsorbed analytes from the adsorbent. Then, it was dried in an oven at 60 °C for 24 h. A new measurement cycle was carried out to determine the adsorption capacity of the regenerated adsorbent.

Results and discussion

Characterization

FTIR

Figure 1 depicts the spectra of (a) β-cyclodextrin, (b) Fe_3O_4, and (c) Fe_3O_4@MAA-βCD recorded in the range of 4000–400 cm^{-1}. The characteristic peaks of β-cyclodextrin appeared at 2927 cm^{-1} due to C–H aliphatic stretching. The absorption band at wavenumber 3325 cm^{-1} indicated –OH stretching (Gao et al. 2017). The peaks at 1632 cm^{-1} and 1614 cm^{-1} are attributed to the presence of coordinated C=O stretching, as shown in spectra (a) and (b) (Paquin et al. 2015). The absorption bands in the 592 cm^{-1} and 586 cm^{-1} range in both spectra (b) and (c) are attributed to the vibrations of Fe–O bonds and proved that the magnetization process of MAA-βCD was successfully done (Almeida Moraes et al. 2020).

SEM

The morphology of the Fe_3O_4 and Fe_3O_4@MAA-βCD was evaluated with SEM. There were considerable dissimilarities in the morphology of the SEM micrographs obtained. The obtained micrographs are shown in

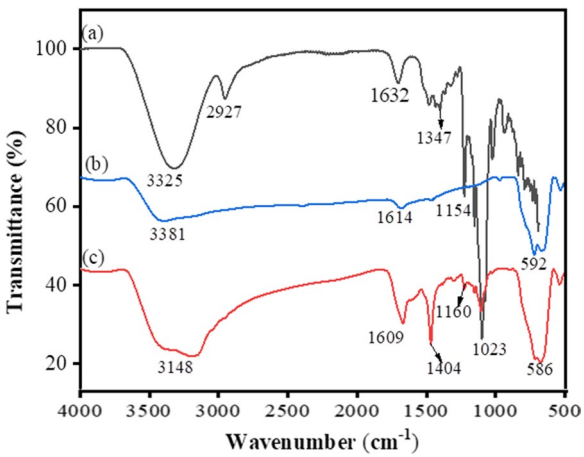

Fig. 1 FTIR spectra of (a) β-cyclodextrin, (b) bare Fe_3O_4, and (c) Fe_3O_4@MAA-βCD

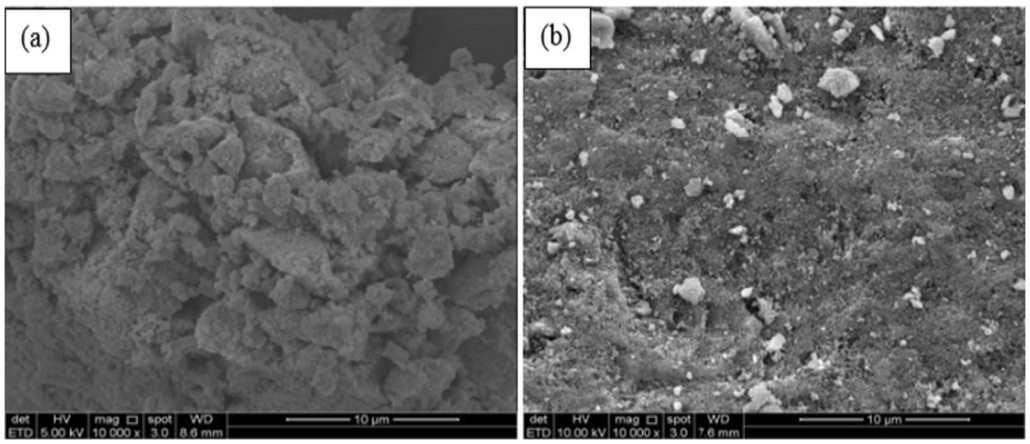

Fig. 2 SEM micrographs of (a) bare Fe_3O_4 and (b) Fe_3O_4@MAA-βCD

Fig. 2. As projected, particles' aggregates were observed due to a large specific surface area-to-volume ratio, resulting in high surface energy for the image of bare Fe_3O_4 in Fig. 2a. The surface of Fe_3O_4@MAA-βCD (Fig. 2b) was seen to be smoother than that of the bare Fe_3O_4. This is because nanoparticles naturally tend to aggregate/agglomeration; modification of their surface or functionalization of polymer chains can prevent the accumulation leading to a smoother surface for Fe_3O_4@MAA-βCD (Ashraf et al. 2018).

VSM

The magnetic properties of bare Fe_3O_4 and Fe_3O_4@MAA-βCD were evaluated by VSM analysis (Fig. 3). The magnetic saturation (*Ms*) values were 80 emu/g (bare Fe_3O_4) and 29 emu g^{-1} (Fe_3O_4@MAA-βCD), respectively. The magnetization obtained in the same field for Fe_3O_4@MAA-βCD was lower. This is primarily ascribed to the presence of β-CD moieties on the surface of the nanoparticles. However, Fe_3O_4@MAA-βCD could be effectively separated from the solution and collected in less than 1 min by an external magnet after the adsorption process.

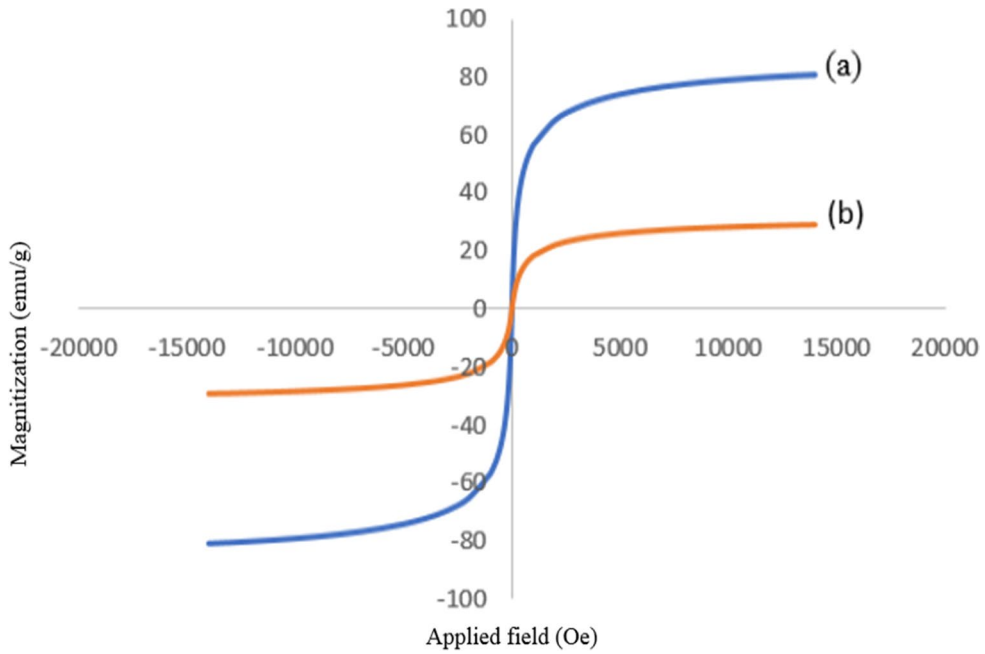

Fig. 3 Magnetization curves of (a) bare Fe_3O_4 and (b) Fe_3O_4@MAA-βCD

This suggests that the material's magnetic strength is sufficient to remove phenolic compounds from aqueous samples.

XRD

XRD analyzed the crystalline pattern of Fe_3O_4 and Fe_3O_4@MAA-βCD; the result is shown in Fig. 4. The results revealed a successful coating of magnetic nanoparticles with MAA-βCD. The nanoparticles' crystal structure is based on Joint Committee on Powder Diffraction Standards, JCPDS 19–0629 (Wardani et al. 2194). Peaks at around $2\theta = 30.46$, 35.73, 43.51, 57.30, and 63.04, which correspond to the crystalline phase of magnetite at (220), (311), (400), (422), and (440) cubic spinal planes of Fe_3O_4, were observed. The intensity of the Fe_3O_4@MAA-βCD peaks was seen to weaken due to the amorphous layer of MAA-βCD.

TEM

TEM (a) image and (b) particle size distribution graph of Fe_3O_4@MAA-β-CD are shown in Fig. 5. Well-shaped spherical or ellipsoidal magnetic nanoparticles were observed. Some small particles aggregate into bigger particles due to their tiny sizes and high surface energy. Furthermore, the images were analyzed using the ImageJ software to determine the particle average particle diameter distribution of the adsorbent materials. Based on the histogram from TEM depicted in Fig. 5b, the particle size's average diameter was between 2 and 50 nm, which falls in the mesoporous range.

Batch adsorption study for the removal of selected phenolic compounds

Effect of pH

pH is one of the most important process variables that can directly influence the analyte's uptake by adsorbents, as it affects the degree of ionization of the analyte and the surface properties of the adsorbent material (Iftekhar et al. 2018). The solution pH is a critical factor in determining the adsorption efficiency of an adsorbent (El-Sayed Eid 2018). This study analyzed the effect of pH on the amount of phenolic compound adsorbed onto Fe3O4@MAA-βCD, as shown in Fig. 6. The removal efficiency of 2,4-DNP over a pH range of 1 to 6 was evaluated and is shown in Fig. 6a. The data obtained reveal that the adsorption was found to be pH-dependent. The removal efficiency increased gradually, and the highest removal percentage was obtained at pH 2 (89%), which was significantly higher than the removal percentage at its natural pH of 4 (76%). In a solution with a low pH, more protons are available to protonate 2,4-DNP (with p*K*a 3.96); hence, the removal efficiency decreases gradually after pH 2. Nevertheless, the protonation of 2,4-DNP was rather difficult since it required very strong acidic

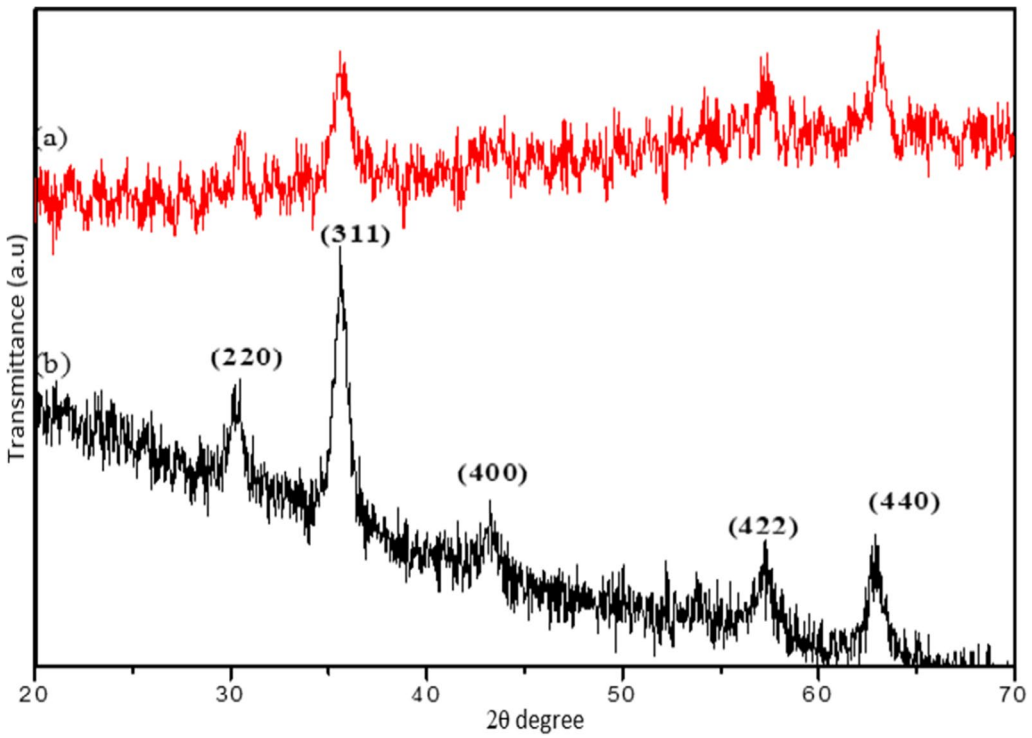

Fig. 4 XRD patterns of (a) Fe_3O_4@ MAA-βCD and (b) bare Fe_3O_4

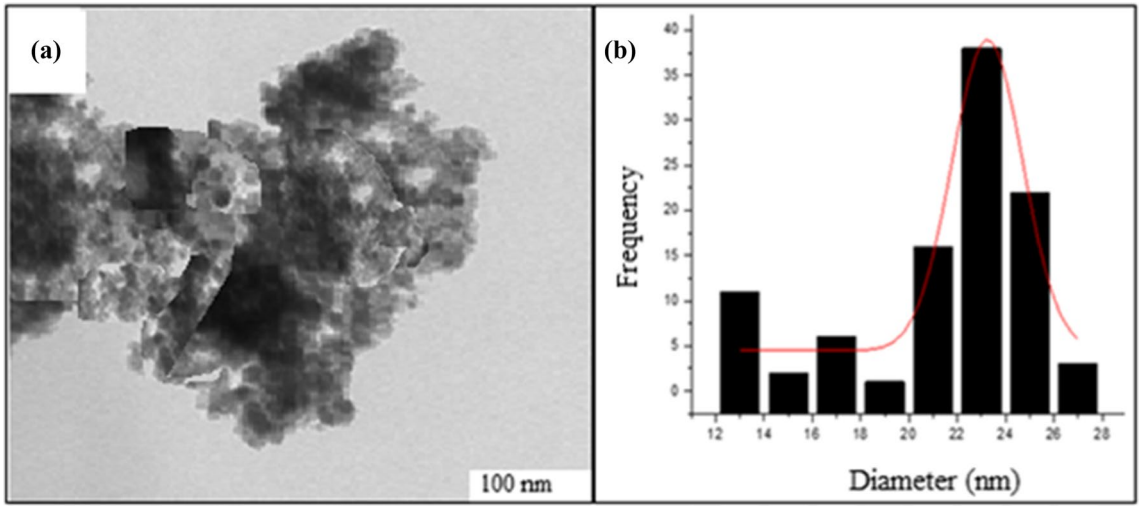

Fig. 5 TEM **a** image and **b** particle size distribution of Fe_3O_4@MAA-βCD

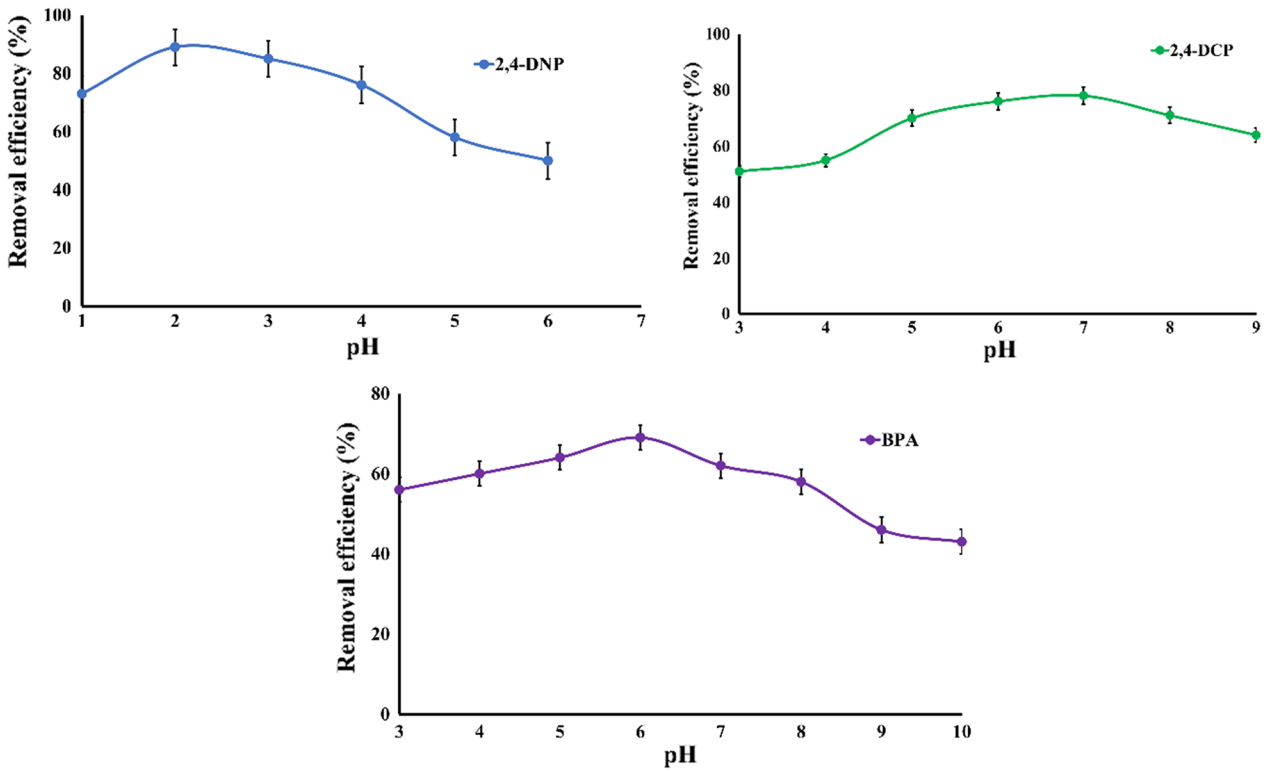

Fig. 6 Effect of pH on the adsorption efficiency of **a** DNP **b** DCP **c** BPA using Fe_3O_4@MAA-βCD as adsorbent. Conditions: (298 K, 10 mL of 10 mg L^{-1} of analyte solution, 20 mg sorbent dose, at 250 rpm shaking speed)

conditions (Anne et al. 2018). When pH < p*K*a, phenolic compounds prefer being in their molecular form, resulting in a low removal capacity at higher pH. Therefore, pH 2 was used as the optimum pH for further studies in this study.

The effect of solution pH on 2,4-DCP adsorption can be discussed as follows: The 2,4-DCP is a hydrophobic organic molecule that can exist in two states in solution: protonated and deprotonated (Magdy et al. 2018). With a pKa of 7.90, 2,4-DCP is a weak acid compound

(Wu et al. 2013). The adsorbed 2,4-DCP was predominantly in the non-ionized form at neutral pH. Hydrophilic analyte molecules (protonated or deprotonated) were unsuitable for forming inclusion complexes with β-CD (Li et al. 2012). As a result, only 2,4-DCP in neutral forms was favored for the inclusion complex formation (Zain et al. 2016). These studies evaluated the effect of pH over a range of 3 to 9. The highest removal efficiency was obtained at pH 7. Afterward, the removal efficiency gradually decreases as the pH increases. It is assumed that the Van der Waals force, the inclusion of complex formation, and bonding hydrogen probably simultaneously dominated the sorption mechanism. Therefore, pH 7 was adopted as an optimized pH for further studies.

The effect of pH on the BPA adsorption was studied from pH 3 to 10, and the highest removal percentage was obtained at pH 6. The removal efficiency decreased gradually until it almost reached equilibrium at pH 9. This could be most likely due to the p*K*a value of BPA. With a pKa of 9.6–10.2, BPA is a weak acid. In an alkaline solution, its particles lose a proton and produce bisphenolate anions. When pH > pKa, BPA adsorption was reduced due to increased repulsion forces and decreased π–π interactions between the adsorbent surface and the bisphenolate anions. The hydroxyl ions compete with BPA molecules at the basic pH range for active sites on the adsorbent surface (Jain et al. 2018; Gao et al. 2017). In this study, therefore, pH 6 was adopted as the pH for further experiments.

Effect of contact time

The effect of contact time for removing phenolic compounds 2,4-DNP, 2,4-DCP, and BPA was studied in the time range of 0–120 min at 298 K, as shown in Fig. 7. The parameters are as follows: the sorbent dose of 20 mg; adsorption time 60 min; temperature 298 K; stirring speed 250 rpm; pH of 2, 7, and 6 for 2,4-DNP, 2,4-DCP, and BPA, respectively, while keeping the initial concentration of 10 mg/L constants for all analytes studied.

The removal of all phenolic compounds increased gradually. The optimum contact time was observed at 60 min, with 89%, 78%, and 69% for 2,4-DNP, 2,4-DCP, and BPA, respectively. The active sites became saturated at 80 min since all samples reached equilibrium. Therefore, in this study, 60 min was chosen as the agitation time for all the analytes studied in subsequent experiments due to the higher removal percentage obtained.

Effect of sorbent dosage

Sorbent dose is an important parameter affecting the sorbate uptake by the sorbent (Badu Latip et al. 2021). To measure the optimum amount of sorbent used in this study, the sorbent dose was varied from 5 to 40 mg, as shown in Fig. 8, while keeping the analytes concentration and contact time constant. The removal efficiency increased slowly when the adsorbent amount was increased from 5 to 20 mg due to the availability of active sites. However, beyond this point, no significant increment was observed for all studied phenolic compounds. Therefore, the sorbent dosage for all analytes studied was fixed at 20 mg for further analysis.

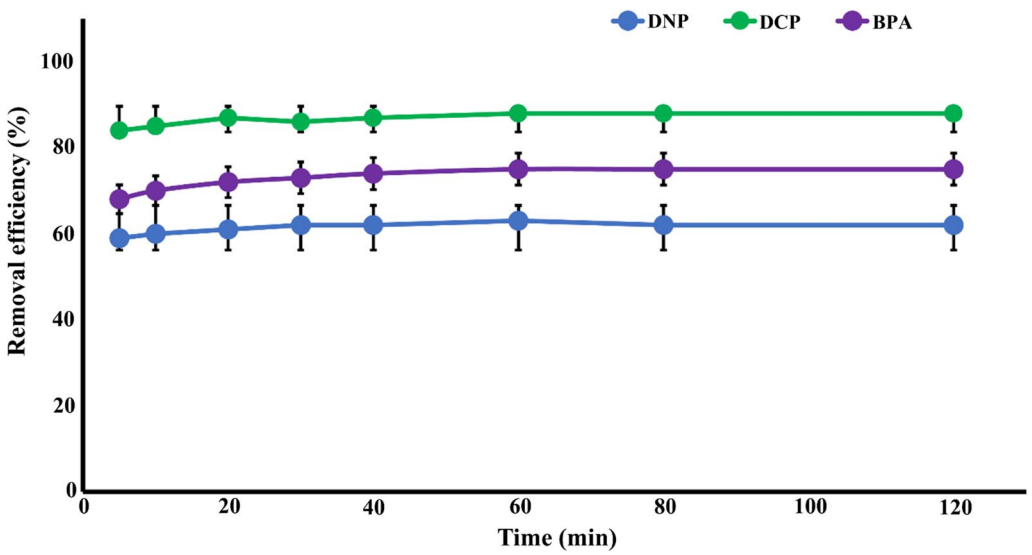

Fig. 7 Effect of contact time on the adsorption efficiency of 2,4-DNP, 2,4-DCP, and BPA. Conditions: (298 K, 10 mL of 10 mg L^{-1} of analyte solution at pH 2, 7, and 6, 20 mg sorbent dose, at 250 rpm shaking speed)

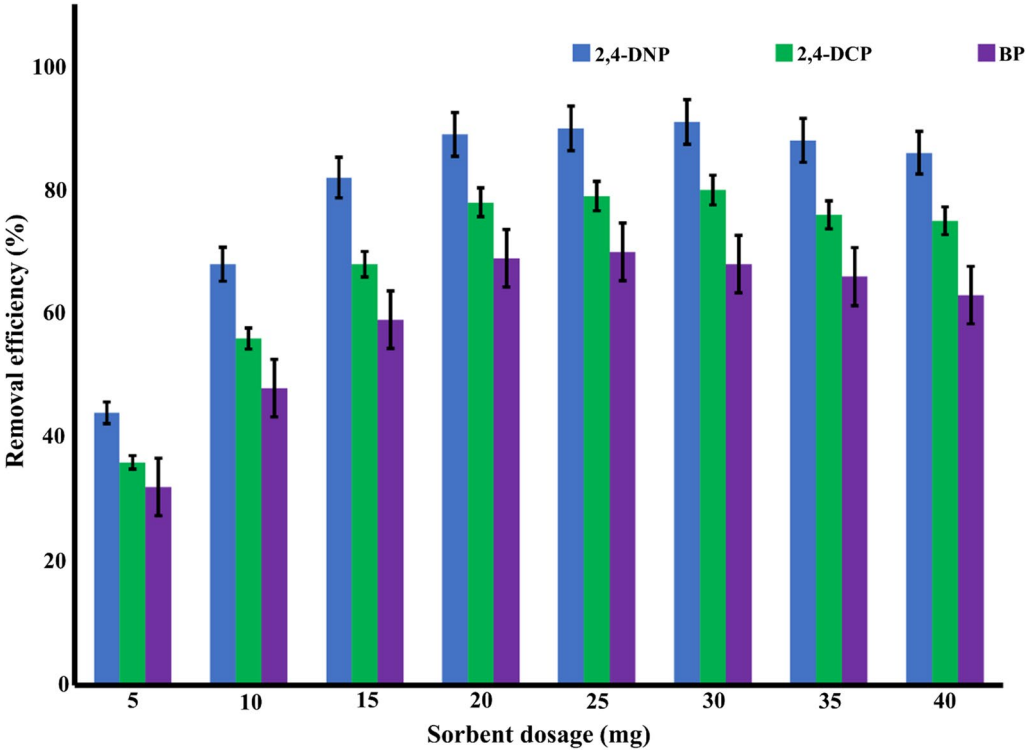

Fig. 8 Effect of sorbent dosage on Fe_3O_4@MAA-βCD. Conditions: (298 K, 10 mL of 10 mg L^{-1} of analyte solution at pH 2, 7, and 6 at 250 rpm shaking speed)

Effect of initial concentration and temperature

The study of temperature and thermodynamics' effect is essential to classify the type of adsorption process (Batool et al. 2018). The experiment was conducted at initial analytes concentrations of 5 mg L^{-1} to 100 mg L^{-1}; sorbent 20 mg; initial concentration of 10 mg L^{-1}; adsorption time 60 min; varying the temperatures to 298 K, 308 K, 318 K, and 328 K; stirring speed 250 rpm; pH of 2,7 and 6 for 2.4-DNP, 2,4-DCP and BPA, respectively. The results obtained are represented in Fig. 9.

The findings revealed that the analytes removal percentage decreased with an increase in the initial concentration due to the limited number of active sites on the surface of Fe_3O_4@MAA-β-CD, leading to the saturation of the analytes at specific concentrations. The temperature has significantly affected the removal performance of all analytes tested. As the temperature rises, the removal efficiency decreases. This finding suggests that all analytes' adsorption on the sorbent is an exothermic process activated more at lower temperatures (Monteiro et al. 2017).

Accuracy of kinetic models

The suitability of the model to describe the adsorption kinetics was further justified and predicated on the normalized standard and relative error (%) as listed in Eq. (3) and Eq. (4).

$$\Delta q(\%) = \sqrt{\frac{\left[\left(q_{\exp} - q_{\mathrm{cal}}\right)/q_{\exp}\right]^2}{N-1}} \times 100 \tag{3}$$

$$\text{Relative error}(\%) = 100\left|\frac{q_{\exp} - q_{\mathrm{cal}}}{q_{\exp}}\right| \tag{4}$$

where N signifies the number of data points, while q_e exp and q_e cal (mg g^{-1}) are the experimental and calculated adsorption capacities, correspondingly. The lower value of Δq and relative error (%) indicates a good fit between observed and calculated data.

Adsorption kinetics

The kinetic study is essential as it provides useful knowledge of the adsorption mechanisms (Abdoli et al. 2015). The pseudo-first-order, pseudo-second-order, Elovich, intraparticle diffusion, and external diffusion models were used to analyze the mass transfer

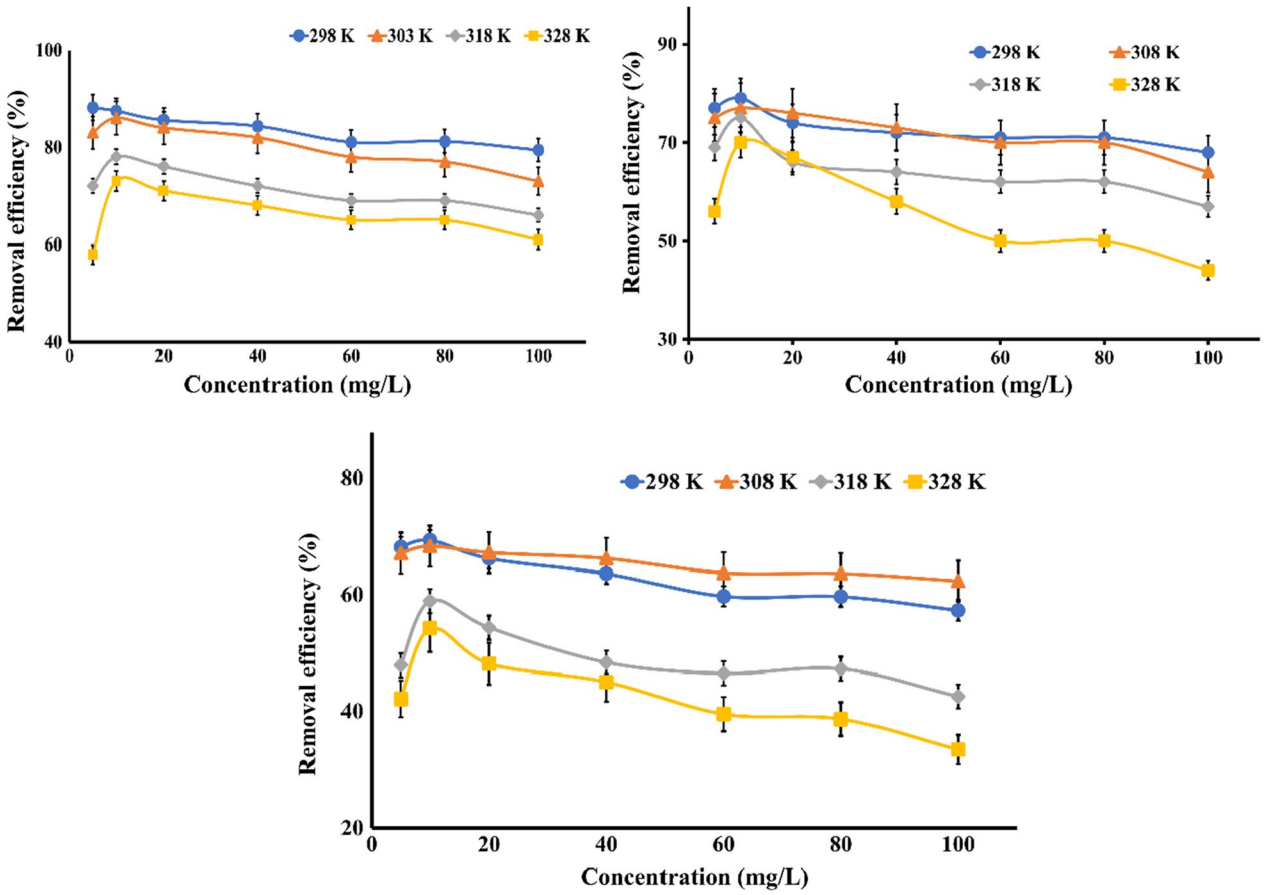

Fig. 9 Effect of initial concentration and temperature on removal of **a** 2,4-DNP, **b** 2,4-DCP, and **c** BPA onto Fe_3O_4@MAA-βCD. Conditions: (298 K, 10 mL of analyte solution at pH 2, 7, and 6, 20 mg sorbent dose, at 250 rpm shaking speed)

mechanism. The linear form of the pseudo-first-order is given as Eq. (5):

$$\log (q_e - q_t) = \log q_e - \frac{k_1}{2.303} t \tag{5}$$

where q_e (mg g^{-1}) is the amount of equilibrium uptake, q_t (mg g^{-1}) is the amount of solute adsorbed at any time t, and k_1 is the rate constant of the pseudo-first-order model (min^{-1}). If the experimental data can be fitted well with pseudo-first order, a straight graph line can be obtained by plotting a graph with a log $(q_e - q_t)$ versus t. In most circumstances, when adsorption is initiated by diffusion across a boundary, the kinetics may follow a pseudo-first-order model. Kinetic parameters calculated from the slope and intercept of the plot are presented in Table 1. The results obtained from this study showed that the pseudo-first-order model is not the best model to describe this adsorption process due to the low R^2, high relative error, and Δq values obtained.

The pseudo-second-order kinetic model is extensively used to analyze adsorption kinetic data. Unlike the pseudo-first-order kinetic model, this model is compatible with the rate-controlling step's mechanism throughout the adsorption process (Ozdes et al. 2014; Phatthanakittiphong and Seo 2016). The linearized form of the pseudo-second-order equation is given as in Eq. (6):

$$\frac{t}{q_t} = \frac{1}{k_2 q_e^2} + \frac{1}{q_e} t \tag{6}$$

whereby plotting a graph of $\frac{t}{q_t}$ versus t gives a straight-line graph with $\frac{1}{q_e}$ and $\frac{1}{k_2 q_e^2}$ as the slope and y-intercept, respectively, if pseudo-second-order is applicable. The value of q_e and k_2 can be obtained directly from the graph without knowing the parameters previously.

The results indicated that the pseudo-second-order model suited better with experimental data for the adsorption of all examined phenolic compounds onto Fe_3O_4@MAA-CD. The studied compounds exhibited a

Table 1 Kinetic parameters for the adsorption of selected phenolic compounds onto Fe_3O_4@MAA-βCD

Kinetic models	Parameters	Analytes		
		2,4-DNP	2,4-DCP	BPA
Pseudo-first-order	q_e exp (mg g^{-1})	5.52721	4.5636	3.3980
	q_e cal (mg g^{-1})	0.2607	0.3125	0.1075
	K_1 (min^{-1})	0.0212	0.0221	0.0484
	R^2	**0.2828**	**0.2445**	**0.0227**
	Δq (%)	35.2082	35.2082	36.6007
	Relative error (%)	95.3213	93.1523	96.8363
Pseudo-second-order	q_e cal (mg g^{-1})	5.5897	4.5914	3.3602
	K_2 (g mg^{-1} min^{-1})	0.1152	0.2602	4.2580
	h (mg g^{-1} min^{-1})	11.3379	5.4855	48.0769
	$t^{1/2}$ (min)	0.0649	0.0567	1.2672
	R^2	**1**	**0.9999**	**0.9999**
	Δq (%)	0.1194	0.2302	0.4205
	Relative error (%)	0.3159	0.6092	1.1124
Elovich equation	q_e cal (mg g^{-1})	5.5512	4.5554	3.3783
	β (g mg^{-1})	12.2249	6.7249	18.6916
	α (mg g min^{-1})	3.0374×10^{26}	3.7480×10^{10}	1.7760×10^{24}
	R^2	**0.9460**	**0.9573**	**0.7121**
	Δq (%)	0.1418	0.0795	0.2204
	Relative error (%)	0.3751	0.1797	0.5778
Intraparticle diffusion	C (mg g^{-1})	5.2952	4.0993	3.2248
	K (mg g min^{-1})	0.0286	0.0505	0.0164
	R^2	**0.8786**	**0.8387**	**0.5114**
External diffusion	K_{ext} (min^{-1})	− 0.0024	− 0.002	− 0.0005
	C (mg g^{-1})	− 1.9118	− 1.2089	− 0.9327
	R^2	**0.7772**	**0.6877**	**0.3237**

The significance of the bold numbers are to highlight the correlation coefficient, R^2 values obtained for each models. These values determine the selection of the model

high coefficient of determination $R^2 \geq 0.9999$ and lower Δq values 2,4-DNP (0.11940), 2,4-DCP (0.2302), and BPA (0.4205), respectively. The adsorption capacity q_e calculated complies with q_e that was obtained from experimental data. This suggests that the adsorption process is predominant and that the overall adsorption process is controlled by chemisorption involving valence through the sharing and exchanging of electrons.

Furthermore, to describe the adsorption process Elovich model was employed. This model presumes that the adsorbate is adsorbed on the solid surface without desorption, and the reductions in adsorption rate with an increase in contact time due to increased surface coverage (Gundogdu et al. 2012) are expressed linearly as in Eq. (7):

$$q_t = \frac{1}{\beta} \ln(\alpha\beta) + \frac{1}{\beta} \ln t \tag{7}$$

where the underlying sorption amount (mg g^{-1} min^{-1}) represented by α, β is identified with the expanded exterior exposure and performing vitality for chemisorption (g^{-1} mg). The plot of q_t versus lnt gives a linear graph with a slope of $\frac{1}{\beta}$ and a y-intercept of $\frac{1}{\beta}\ln(\alpha\beta)$ respectively. The $\frac{1}{\beta}$ value reflects the number of sites available for adsorption, whereas the value of $\frac{1}{\beta}\ln(\alpha\beta)$ shows the adsorption quantity when lnt is equal to zero.

The external diffusion and intraparticle diffusion models were applied to determine the real mass transfer constraint limiting the adsorption of the targeted phenolic chemicals. According to the external diffusion model, the adsorbent surface concentration approaches zero. The intraparticle resistance is very small, and the intraparticle diffusion at initial contact times can be ignored (Luz-Asunción et al. 2015). If the transition of solute molecules from the liquid to the solid phase plays an important role in the adsorption process, the liquid film diffusion model can be applied. The external diffusion model is defined as in Eq. (8):

$$ln\frac{C_t}{C_0} = -K_{\text{ext}}t \tag{8}$$

where C_o and C_t indicate the concentration of the solute in the liquid phase at the time, t and K_{ext} (min^{-1}) is a diffusion rate parameter. The plot of $ln\ \frac{C_t}{C_0}$ against t should give a linear line with zero intercepts if the external diffusion is applicable (G. qian Wu et al. 2013; Badu Latip et al. 2021; Batool et al. 2018; Ozdes et al. 2014; Phatthanakittiphong and Seo 2016).

Weber and Morris consider intraparticle diffusion as the rate-controlling step for adsorption. The intraparticle diffusion model is expressed as Eq. (9):

$$q_t = Kt^{0.5} + c \tag{9}$$

where K is the intraparticle diffusion rate constant ($mg\ g^{-1}\ min^{0.5}$) and c represent the y-intercept ($mg\ g^{-1}$). The q_t ($mg\ g^{-1}$) is the amount adsorbed at time t (min).

The value of c gives an idea of the thickness of the boundary layer. The higher the c value, the greater the boundary effect and hence better adsorption of the studied compounds. The results obtained showed that the value of c was in the order of 2,4-DNP (5.2952) > 2,4-DCP (4.0993) > BPA (3.2248). Meanwhile, the values of R^2, i.e., 0.9460 (2,4-DNP), 0.9573 (2,4-DCP), and 0.7121 (BPA), respectively, were also obtained. The intercept c does not pass through the origin of the received data, suggesting that intraparticle diffusion is not the only rate-controlling.

The kinetic data fitted in the order of second order > Elovich > intraparticle diffusion > external diffusion > first order. The models' validity was compared using R^2 values, normalized standard deviation (%), and relative error (%), as illustrated in Table 1.

Adsorption isotherm models

Adsorption isotherm was investigated to explain the adsorbent interactive behavior at a given temperature on the adsorbent surface. Five isotherm models were studied, the linear form of Langmuir, Freundlich, Temkin, Halsey, and Dubinin–Radushkevich. The experimental equilibrium data at four different temperatures (298 K, 308 K, 318 K, and 328 K) were calculated, and the values of the isotherm model constant with their respective correlation coefficients are presented in Table 2.

The Langmuir isotherm assumes that the adsorption process is uniformly distributed within the adsorbent surface and has uniform energy levels (Girish and Murty 2016; Shahriman et al. 2018). This model can be used to elucidate the adsorption of phenolic compounds from aqueous solutions (Davidescu et al. 2019). The linear form of the Langmuir isotherm is given as in Eq. (10):

$$\frac{1}{q_e} = \frac{1}{bq_e} + \frac{C_e}{q_m} \tag{10}$$

where C_e($mg\ L^{-1}$) is the equilibrium concentration of the adsorbate, q_e ($mg\ g^{-1}$) is the amount of adsorbate adsorbed per specific amount of adsorbate, q_m($mg\ g^{-1}$) and b ($L\ mg^{-1}$) are Langmuir consistent identified with the adsorption limit and the rate of adsorption, separately. Furthermore, to evaluate whether the adsorption process is favorable, the dimensionless separation factor (R_L) can be calculated from Eq. (11):

$$R_L = \frac{1}{1 + bC_0} \tag{11}$$

The value of $R_L = 0$ applies for irreversible adsorption, $0 < R_L < 1$ for favorable adsorption $R_L = 1$ for linear and $R_L > 1$ for unfavorable equilibrium.

The interaction between adsorbate and adsorbent at equilibrium was assessed by the coefficient of determination (R^2), which is $R^2 > 0.8158$, except for BPA at 328 K with R^2 of 0.1101. This could be because of its lower hydrophobicity and higher temperature; hence, BPA could not interact with the cavity of β-CD. Therefore, the Langmuir model was not the best to describe the adsorption of 2,4-DNP, 2–4 DCP, and BPA onto Fe_3O_4@MAA-βCD.

Freundlich isotherm can be applied to multilayer adsorption and heterogeneous surfaces with non-uniform distribution of adsorption heat (Theydan and Ahmed 2012). The linear form of the Freundlich isotherm is expressed as Eq. (12):

$$\log q_e = \log fK_F + \frac{1}{n_F}\log C_e \tag{12}$$

where K_F is the adsorption capacity (($mg\ g^{-1}$) ($L\ mg^{-1}$)$^{1/n}$), while the Freundlich constant is characterized by n, separately. A larger value of K_F points to greater adsorption capacity, while n_F values designate the preferability of the adsorption process. The adsorption process is favorable for physical adsorption if n_F is above unity (Magdy et al. 2018).

To account for the multilayer adsorption, the linear plot of the Freundlich model was used. It best fitted the experimental data with $R^2 > 0.9374$ for the studied analytes at 298 K, 308 K, 318 K, and 328 K. Numerous studies have found that the adsorption process of phenolic compounds is best fitted by the Freundlich isotherm (Luz-Asunción et al. 2015; Girish and Murty 2016). This indicates that the adsorption occurred on a heterogeneous surface (Surikumaran et al. 2015). The value of n, which is a pointer for adsorption intensity, was more than unity, indicating favorable adsorptions for all studied adsorbates. The K_F

Table 2 Details of isotherm constants for the adsorption of selected phenolic compounds onto Fe_3O_4@MAA-βCD

Isotherm models	Parameters	298 K	308 K	318 K	328 K
2,4-DCP					
Langmuir	q_m (mg g^{-1})	74.5475	72.9927	64.1026	36.3636
	b (L mg^{-1})	0.3951	0.0234	0.0192	0.0267
	R^2	**0.9535**	**0.6150**	**0.6346**	**0.7792**
	R_L	0.0119	0.0163	0.0164	0.0162
Freundlich	K_F (mg g^{-1}) (L mg^{-1})$^{1/n}$	1.7571	1.6235	1.4478	1.2294
	N	1.1497	1.1833	1.2223	1.3330
	$1/n$	0.8698	0.8451	0.8182	0.7502
	R^2	**0.9969**	**0.9768**	**0.9750**	**0.9620**
Temkin	K_T (L mg^{-1})	0.6499	0.6638	0.5573	0.5163
	b_T (kJ mol^{-1})	257.7636	276.3915	329.4766	449.4295
	R^2	**0.9189**	**0.9058**	**0.9346**	**0.9670**
Dubinin–Radushkevich	q_m (mg g^{-1})	18.6734	18.7670	16.7584	15.3990
	β (L mg^{-1})	1.0974	1.1015	1.3011	2.2853
	R^2	**0.7684**	**0.8048**	**0.8604**	**0.8962**
	E	0.6750	0.6737	0.6199	0.4677
Halsey	N	− 1.1497	− 1.1833	− 1.2222	− 1.3165
	K_H	0.5230	0.5012	0.6362	0.7740
	R^2	**0.9535**	**0.6150**	**0.6346**	**0.7792**
2,4-DNP					
Langmuir	q_m(mg g^{-1})	80.0000	67.5676	80.6452	62.2903
	b (L mg^{-1})	0.0438	0.0427	0.0199	0.0064
	R^2	**0.9396**	**0.9417**	**0.8158**	**0.1101**
	R_L	0.016	0.0159	0.0163	0.0166
Freundlich	K_F (mg g^{-1}) (L mg^{-1})$^{1/n}$	3.5449	2.9512	1.7354	1.0980
	n	1.2355	1.2475	1.1671	0.9467
	$1/n$	0.8094	0.8016	0.8568	0.5797
	R^2	**0.9983**	**0.9830**	**0.9842**	**0.9542**
Temkin	K_T (L mg^{-1})	1.2686	1.0368	0.6423	0.4624
	b_T (kJ mol^{-1})	241.974	262.0056	284.9992	288.595
	R^2	**0.9100**	**0.9529**	**0.9402**	**0.9572**
Dubinin–Radushkevich	q_m(mg g^{-1})	22.2646	21.1979	19.8142	20.1640
	β (L mg^{-1})	0.6691	0.4505	1.2056	2.3790
	R^2	**0.7676**	**0.8657**	**0.8647**	**0.9116**
	E	0.8644	1.0535	0.6439	0.4584
Halsey	N	− 1.2355	− 1.2475	− 1.1671	− 1.0563
	K_H	0.2094	0.2592	0.6236	0.9153
	R^2	0.9983	0.9830	0.9842	0.9542
BPA					
Langmuir	q_m(mg g^{-1})	68.0272	75.7576	60.6061	76.9231
	b (L mg^{-1})	0.0162	0.0158	0.0098	0.0139
	R^2	**0.8658**	**0.8658**	**0.8416**	**0.8348**
	R_L	0.0164	0.0158	0.0165	0.0164
Freundlich	K_F (mg g^{-1}) (L mg^{-1})$^{1/n}$	1.2756	1.3677	0.6901	0.6148
	n	1.1898	1.1525	1.1457	1.2099
	$1/n$	0.8405	0.8677	0.8728	0.8265
	R^2	**0.9948**	**0.9892**	**0.9852**	**0.9874**

Table 2 (continued)

Isotherm models	Parameters	298 K	308 K	318 K	328 K
Temkin	K_T (L mg^{-1})	0.4930	0.4890	0.3384	0.3312
	b_T (kJ mol^{-1})	306.5467	282.986	410.4659	534.0969
	R^2	**0.9017**	**0.9394**	**0.9133**	**0.9724**
Dubinin–Radushkevich	q_m (mg g^{-1})	15.2646	17.542	13.2965	11.5791
	β (L mg^{-1})	1.8928	1.774	3.4798	4.5764
	R^2	**0.7747**	**0.8018**	**0.8065**	**0.9178**
	E	0.5140	0.5309	0.3791	0.3305
Halsey	N	− 1.1898	− 1.1525	− 1.1457	− 1.2099
	K_H	0.7486	0.6971	1.2027	1.2914
	R^2	**0.9948**	**0.9892**	**0.9852**	**0.9874**

The significance of the bold numbers are to highlight the correlation coefficient, R^2 values obtained for each models. These values determine the selection of the model

values for 2,4-DNP at all studied temperatures were more extensive than all other phenolic compounds studied, suggesting that it has superior adsorption capacity and had more heterogeneous binding sites. Also, the reduction in K_F value with a rise in temperature shows the adsorption process's exothermic phenomena.

The heat of adsorption and the adsorption binding energy are explored by the Temkin Eqs. (13–14) as follows:

$$q_e = \beta \ln K_T + \beta \ln C_e \tag{13}$$

$$\beta = \frac{RT}{b_T} \tag{14}$$

where q_e is the amount of adsorbate adsorbed at equilibrium (mg g^{-1}), C_e is the concentration of the adsorbate at equilibrium (mg L^{-1}), K_T refers to the isotherm intercept (mg L^{-1}), and b_T denotes the heat of adsorption. The graph for this model was plotted for q_e against ln C_e.

In this study, the Temkin model gave the R^2 values in the range of 0.8950–0.9749 for the studied analytes. The heat of sorption (kJ mol^{-1}) increased as the temperature increased in the order of 2,4-DNP (241.974–288.595), 2,4-DCP (257.7636–449.4295), and BPA (306.547–534.0969) as given in Table 2.

The Dubinin–Radushkevich model is frequently used to evaluate the characteristic porosity and the apparent free energy of adsorption (Ozdes et al. 2014). This can be expressed in Eq. (15) and Eq. (16):

$$\ln q_e = \ln q_m - \beta E^2 \tag{15}$$

$$E = RT \ln[1 + 1/C_e] \tag{16}$$

where q_e represents the adsorption capacity (mg g^{-1}), q_m is the theoretical saturation capacity (mg g^{-1}), and β denotes the adsorption energy constant. E is the mean adsorption-free energy, C_e is the equilibrium concentration of phenolic compounds in solution (mol L^{-1}), R (8.314 kJ mol^{-1}) is the gas constant, and T (K) is the absolute temperature.

D-R isotherm model is principally applied to express the adsorption mechanism with a Gaussian energy distribution onto a heterogeneous surface (Surikumaran et al. 2015). E is related to the free energy of adsorption per adsorbate when transferred to the solid surface from infinity in the solution, enabling the prediction of the adsorption type (Girish and Ramachandra Murty 2014) since the E values were all small in Table 2. A possible physisorption process between adsorbent and adsorbate is proposed for this study.

Finally, the Halsey isotherm model was used to assess multilayer adsorption at a relatively large distance from the surface (Mahmad et al. 2030). The adsorption isotherm can be given as Eq. (17):

$$\ln q_e = \left[\frac{1}{n} \ln K_H\right] - \frac{1}{n} \ln C_e \tag{17}$$

where q_e is equal to adsorption capacity (mg g^{-1}), C_e represents the equilibrium concentration, and K_H is the Halsey isotherm constant. The linear plot of the graph ln q_e versus *In* C_e indicates the degree of heteroporosity of adsorbents.

Based on the results, the R^2 values for all studied phenolic compounds were > 0.9058. This attests to the fact that Fe_3O_4@MAA-βCD has a heterosporous structure, and multilayer adsorption was involved during the removal process.

Thermodynamic studies

The values of thermodynamic parameters such as enthalpy change, Gibbs free energy, and entropy change give an idea of the spontaneity of the adsorption process and can be expressed as in Eq. (18–20):

$$\Delta G^{\circ} = -RT \ln k_d \tag{18}$$

$$\ln k_d = \frac{\Delta S^o}{R} - \frac{\Delta H^o}{RT} \tag{19}$$

$$k_d = \frac{q_e(\text{equillibrium adsorbate in adsorbent})}{C_e(\text{equillibrium adsorbate in solution})} \tag{20}$$

where ΔG° is Gibbs free energy, R is a universal gas constant, kJ (mol k^{-1}), T is the temperature (K), while k_d is the equilibrium constant. The ΔS° is the entropy change in the system; the ΔH° is the enthalpy ratio of the concentration of adsorbate on adsorbent at equilibrium. q_e is the adsorption capacity (mg g^{-1}), and C_e is the adsorbate remaining concentration in solution at equilibrium.

Data from the slope and intercept of the thermodynamic plot (Van't Hoff's plot) were calculated for the feasibility of 2,4-DNP, 2,4-DCP, and BPA adsorption. The values of ΔG°, ΔH°, and ΔS° are given in Table 3. The data obtained values of ΔH° were found to be − 24.00, − 25.69, and − 15.44 J mol^{-1} for 2,4-DNP, 2,4-DCP, and BPA, respectively. The negative ΔH° values confirm that the adsorption mechanism is an exothermic reaction. This finding is supported by the decrease in K_F value uptake capacity of the adsorbent as the temperature increases (Dada et al. 2017).

On the other hand, the negative values of ΔS° obtained for all the studied analytes (− 74.11, − 83.41, and − 55.46) indicate the point to a decrease in the degree of randomness at the adsorbent/solution interface during the adsorption process. Generally, the adsorption process is spontaneous when the values of ΔG° are negative (Tahermansouri et al. 2015). The value of Gibb's free energy ΔG° is negative at a given temperature; however, in this study, the thermodynamic data for BPA were found to be positive and weak ΔH° value. Therefore, it can be deduced that the adsorption process is feasible but not spontaneous. The thermodynamic data recorded for 2,4-DNP and 2,4-DCP in Table 3 showed that the adsorption process is exothermic and might be spontaneous at lower temperatures.

Table 3 Thermodynamic parameters of studied phenolic compounds onto Fe_3O_4@MAA-βCD

Analytes	T (K)	Gibbs energy, ΔG° kJ mol^{-1}	Enthalpy, ΔH° J mol^{-1}	Entropy, ΔS° kJ mol^{-1}
2,4-DNP	298	− 19.11	− 24.00	− 74.11
	308	− 12.87		
	318	− 22.20		
	328	19.59		
2,4-DCP	298	− 51.12	− 25.69	− 83.41
	308	− 36.86		
	318	50.62		
	328	20.37		
BPA	298	17.49	− 15.44	− 55.46
	308	62.86		
	318	22.02		
	328	31.47		

Real samples analysis for the removal of selected phenolic compounds

The practical applicability of the process developed for removing the phenolic compound was evaluated using reproducibility, precision, and removal studies. Firstly, the calibration curve was prepared for the removal procedure under optimized conditions of all parameters tested. Serial dilutions determined the linear range of phenolic compounds at different concentration levels. Reproducibility and accuracy of the proposed method are presented as inter-day and intraday in terms of relative standard deviation (RSD) and were tested by triplicate determinations using low, medium, or high concentrations (1, 10 and 60 mg L^{-1}). For intraday triplicate determination for each vial, each concentration level was conducted in seven separate vials ($n=6$). Thus, similar procedures were followed for inter-day intervals for four consecutive days skipping one day and completing the last removal on the sixth day ($n+5$) to obtain the percentage removal and (RSD %) values. Four water samples from different sources under the optimum adsorbate conditions spiked at different concentrations. The summary of the obtained results is given in Table 4. The repeatability and reproducibility of the removal were determined intraday and inter-day using triplicate determination. The precision was expressed as the relative standard deviation, ranging from 0.12 to 4.23% for all studied phenolic compounds. The percentage removal of phenols is presented in Table 5 in the range of 61.70–69.40% for BPA, 71.40–79.30% for 2,4-DCP, and 86.3–89.4% for 2,4-DNP, respectively. These results indicate good reproducibility and repeatability; therefore, the developed method has been proven applicable to real matrix applications.

Table 4 Analytical performance data for the removal of selected phenolic compounds using UV–Vis spectrophotometry

Analytes	Regression equation	R^2	Spiked concentrations (mg L^{-1})	Intraday ($n=5$)		Inter-day ($n=6$)	
				Removal (%)	RSD (%)	Removal (%)	RSD (%)
BPA	$y=0.0156x+0.040$	0.9997	1	64.33	1.85	67.59	4.20
			10	69.34	0.71	69.14	1.36
			60	68.39	1.21	67.12	0.74
2,4-DNP	$y=0.0157x+0.0709$	0.9999	1	86.76	0.12	87.45	3.91
			10	89.42	1.13	89.33	4.23
			60	88.63	1.18	87.82	1.83
2,4-DCP	$y=0.0282x+0.1438$	0.9992	1	75.55	3.54	74.35	1.96
			10	77.61	1.27	78.06	1.47
			60	75.78	1.66	76.91	3.65

Table 5 Removal (%) and RSD ($n=3$) of real sample for the removal of phenols by Fe_3O_4@ MAA-βCD

Water sample		Tap water	Rubber industry	Plastic industry	Wooden industry
Phenolic compounds	Spiked concentration (mg L^{-1})	Removal (%) ± RSD	Removal (%) ± RSD	Removal (%) ± RSD	Removal (%) ± RSD
BPA	1	69.4 ± 0.2	64.6 ± 5.5	66.4 ± 2.3	67.2 ± 3.8
	10	68.0 ± 1.2	67.3 ± 2.0	69.4 ± 1.6	67.2 ± 2.3
	60	61.7 ± 2.6	66.7 ± 1.7	68.4 ± 0.2	67.8 ± 1.3
2,4-DCP	1	79.3 ± 0.6	74.1 ± 6.9	75.1 ± 5.6	76.2 ± 1.7
	10	78.7 ± 1.7	77.1 ± 2.5	74.7 ± 2.1	76.9 ± 4.9
	60	77.8 ± 0.5	77.7 ± 1.5	77.3 ± 1.2	76.7 ± 0.4
2,4-DNP	1	86.4 ± 0.3	88.4 ± 0.4	89.4 ± 4.1	88.9 ± 3.8
	10	86.3 ± 0.2	87.2 ± 0.1	86.5 ± 2.1	87.4 ± 1.4
	60	89.4 ± 0.3	88.8 ± 0.9	86.4 ± 0.2	88.1 ± 1.4

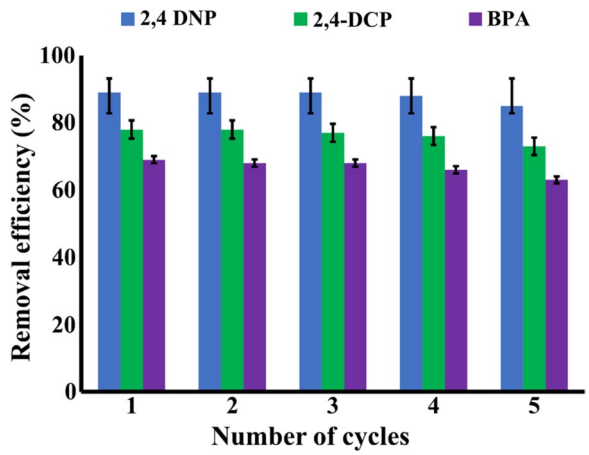

Fig. 10 Fe_3O_4@MAA-βCD for the removal of selected phenolic compounds. Conditions: (298 K, 10 mL of analyte solution (10 mg L^{-1}) at pH 2, 7, and 6, 20 mg sorbent dose, and 60 min shaking time at 250 rpm)

Reusability study of Fe_3O_4@MAA-βCD for the removal of selected phenolic compounds

Recycling any adsorbent is significant as a cost-effective water treatment process (Gopal et al. 2019). Reusability analysis was conducted to study the reusability of the adsorbent. The study was carried out by subjecting the same Fe_3O_4@MAA-βCD adsorbent over five cycles to examine the removal efficiency. The results indicated that Fe_3O_4@MAA-βCD is a feasible renewable adsorbent since, even after five successive cycles, there was no significant reduction in the removal percentage, as shown in Fig. 10.

Comparison of adsorbent

In Table 6, a comparison between the adsorption capacity (q_e), removal efficiency, various optimization settings, and models that best represent their

Table 6 Comparison of adsorbent used in this study with other adsorbents used for the removal of phenolic compounds

Adsorbents	Adsorbate	Adsorption capacity (q_m) mg/g	References
Molecular imprinted polymer of methacrylic acid-functionalized beta-cyclodextrin (MIP-MAA/β-CD)	2,4-DCP	45.7	Surikumaran et al. (2014)
Fe_3O_4@AC–SS	2,4-DCP	98.0	Gopal et al. (2019)
	2,4-DNP	46.1	
Activated carbon-impregnated alginate*β-cyclodextrin/gelatin beads	2,4-DCP	39.4	Alsohaimi et al. (2020)
Molecularly imprinted thiol-functionalized activated titanium dioxide	2,4-DNP	16.5	Zhou et al. (2018)
Titania–silica mixed imidazolium-based ionic liquid	2,4-DNP	7.78	Ismail et al. (2016)
Film-like bacterial cellulose/cyclodextrin oligomer composites	BPA	34.1	Liu et al. (2021)
	2,4-DCP	92.9	
β-CD grafted cellulose bead	BPA	30.7	Lin et al. (2019)
β-CD-modified graphene oxide membranes	BPA	25.5	Chen et al. (2020)
Zeolite from fly ash modified with β-CD	BPA	33.8	Bandura et al. (2021)
Imidazolium ionic liquids on silica	2,4-DNP	57.9	Wang et al. (2019)
Fe_3O_4@ MAA-β-CD	BPA	68.0	This work
	2,4-DNP	80.0	
	2,4-DCP	74.6	

adsorption by various sorbents utilized to remove phenolic compounds in the literature is made. This research is comparable to previous studies on removing phenolic chemicals using various adsorbents. As a result, Fe_3O_4@MAA-βCD may be considered a potential adsorbent for phenolic compound removal from aqueous solutions.

Conclusion

Fe_3O_4@MAA-βCD was successfully synthesized in this work, characterized and applied as an adsorbent to remove some selected phenolic compounds from aqueous media. The optimal removal amount of phenolic compounds studied was obtained at pH 2 for 2,4-DNP, pH 7 for 2,4-DCP, and pH 6 for BPA. At the same time, the contact time, initial concentration, and the adsorbent dose were set at 60 min, 10 mg L^{-1}, and 20 mg, respectively. The adsorption isotherm data indicated that the surface Fe_3O_4@MAA-βCD was multilayered. Hence, Freundlich and Halsey's isotherm models were the best models to describe the adsorption process. The adsorption kinetic processes followed the pseudo-second-order kinetics, and the intraparticle diffusion results reveal that the adsorption mechanism involved more than one approach. The thermodynamic data showed that the adsorption process was exothermic and spontaneous, and a lower temperature favored the adsorption. It is suggested that the inclusion complex formation, π–π interactions stacking interaction, and hydrogen bonding were the main types of interaction governing the studied analytes' adsorption onto Fe_3O_4@MAA-βCD. This material can be reused for up to five successive cycles. Consequently, this adsorbent is a low-cost and efficient material with excellent potential for removing phenolic compounds from aqueous media.

Acknowledgements
The authors would like to seize this opportunity to express their gratitude to Fundamental Research Scheme, Ministry of Higher Education (MOHE), Malaysia (FRGS; Reference code: FRGS/1/2018/STG01/USM/03/4, Account no.: 203.CIPPT.6711661), for the assistance and financial support. The authors also acknowledge the Advanced Medical and Dental Institute and School of Chemical Science, Universiti Sains Malaysia, for the facilities provided.

Author contributions
MS contributed to writing—original draft preparation, methodology, and software. SFF bin SY contributed to writing—reviewing and editing, data curation, and formal analysis. MR contributed to methodology and supervision. FS contributed to software and project administration. NNMZ contributed to funding acquisition, conceptualization, and supervision. FBMS contributed to conceptualization, visualization, and supervision. All authors read and approved the final manuscript.

Funding
The authors would like to seize this opportunity to express their gratitude to Fundamental Research Scheme, Ministry of Higher Education (MOHE), Malaysia (FRGS; Reference code: FRGS/1/2018/STG01/USM/03/4), for financial support.

Availability of data and materials
Almost all details are presented and cited in the article.

Declarations

Ethics approval and consent to participate.
The manuscript does not contain clinical or trial studies on patients, humans, or animals.

Consent for publication
All authors have given consent for publication.

Competing interests
The authors declare that they have no known competing financial interests or personal relationships that could have appeared to influence the work reported in this paper.

Received: 27 October 2022 Accepted: 5 January 2023
Published online: 13 January 2023

References

Abdel-Ghani NT, Rawash ESA, El-Chaghaby GA. Equilibrium and kinetic study for the adsorption of p-nitrophenol from wastewater using olive cake based activated carbon. Glob J Environ Sci Manag. 2016;2:11–8. https://doi.org/10.7508/gjesm.2016.01.002.

Abdoli SM, Bastani D, Bargozin H. Adsorption of phenol compounds by nanoporous silica aerogel. Sci Iran. 2015;22:992–1000.

Allaboun H, Abu Al-Rub FA. Removal of 4-chlorophenol from contaminated water using activated carbon from dried date pits: equilibrium, kinetics, and thermodynamics analyses. Materials. 2016;9:251–65. https://doi.org/10.3390/ma9040251.

Almeida Moraes T, Farrôco MJ, Pontes K, Fontes Bittencourt M, Guenter Soares B, Gomes Souza F. An optical-magnetic material as a toxic gas filter and sensing device. RSC Adv. 2020;10:23233–44. https://doi.org/10.1039/d0ra00537a.

Alsohaimi IH, El-Aassar MR, Elzain AA, Alshammari MS, Ali ASM. Development of activated carbon-impregnated alginate*β-cyclodextrin/gelatin beads for highly performance sorption of 2,4-dichlorophenol from wastewater. J Mater Res Technol. 2020;9:5144–53. https://doi.org/10.1016/j.jmrt.2020.03.031.

Anne JM, Boon YH, Saad B, Miskam M, Yusoff MM, Shahriman MS, Zain NNM, Lim V, Raoov M. β-Cyclodextrin conjugated bifunctional isocyanate linker polymer for enhanced removal of 2,4-dinitrophenol from environmental waters. R Soc Open Sci. 2018. https://doi.org/10.1098/rsos.180942.

Ashraf MA, Peng W, Zare Y, Rhee KY. Effects of size and aggregation/agglomeration of nanoparticles on the interfacial/interphase properties and tensile strength of polymer nanocomposites. Nanoscale Res Lett. 2018;13:1–7. https://doi.org/10.1186/s11671-018-2624-0.

Asiri AM, Akhtar K, Seo J, Marwani HM, Kim D, Han H, Khan SB. Development of polymer based nanocomposites as a marker of cadmium in complex matrices. J Nanomater. 2015. https://doi.org/10.1155/2015/942756.

Badu Latip NM, Gopal K, Suwaibatu M, Hashim NM, Rahim NY, Raoov M, Yahaya N, Mohamad Zain NN. Removal of 2,4-dichlorophenol from wastewater by an efficient adsorbent of magnetic activated carbon. Sep Sci Technol. 2021;56:252–65. https://doi.org/10.1080/01496395.2020.1719156.

Balci B, Erkurt FE. Adsorption of Bisphenol-A by eucalyptus bark/magnetite composite: modeling the effect of some independent parameters by multiple linear regression. Adsorpt Sci Technol. 2017;35:339–56. https://doi.org/10.1177/0263617416676819.

Bandura L, Białoszewska M, Malinowski S, Franus W. Adsorptive performance of fly ash-derived zeolite modified by β-cyclodextrin for ibuprofen, bisphenol A and caffeine removal from aqueous solutions—equilibrium and kinetic study. Appl Surf Sci. 2021. https://doi.org/10.1016/j.apsusc.2021.150160.

Batool F, Akbar J, Iqbal S, Noreen S, Bukhari SNA. Study of isothermal, kinetic, and thermodynamic parameters for adsorption of cadmium: an overview of linear and nonlinear approach and error analysis. Bioinorg Chem Appl. 2018;2018:1–11. https://doi.org/10.1155/2018/3463724.

Biglari H, Afsharnia M, Alipour V, Khosravi R, Sharafi K, Mahvi AH. A review and investigation of the effect of nanophotocatalytic ozonation process for phenolic compound removal from real effluent of pulp and paper industry. Environ Sci Pollut Res. 2017;24:4105–16. https://doi.org/10.1007/s11356-016-8079-x.

Bohdziewicz J, Kamińska G, Tytła M. The removal of phenols from wastewater through sorption on activated carbon. Archit Civ Eng Environ. 2012;2:89–94.

Chen ZH, Liu Z, Hu JQ, Cai QW, Li XY, Wang W, Faraj Y, Ju XJ, Xie R, Chu LY. β-Cyclodextrin-modified graphene oxide membranes with large adsorption capacity and high flux for efficient removal of bisphenol A from water. J Memb Sci. 2020;595:117510–7. https://doi.org/10.1016/j.memsci.2019.117510.

Dada AO, Adekola FA, Odebunmi EO. A novel zerovalent manganese for removal of copper ions: synthesis, characterization and adsorption studies. Appl Water Sci. 2017;7:1409–27. https://doi.org/10.1007/s13201-015-0360-5.

Davidescu CM, Ardelean R, Popa A. New polymeric adsorbent materials used for removal of phenolic derivatives from wastewaters. In: Pure Appl Chem, 2019. pp. 443–458. https://doi.org/10.1515/pac-2018-1019.

De La Luz-Asunción M, Sánchez-Mendieta V, Martínez-Hernández AL, Castaño VM, Velasco-Santos C. Adsorption of phenol from aqueous solutions by carbon nanomaterials of one and two dimensions: kinetic and equilibrium studies. J Nanomater. 2015. https://doi.org/10.1155/2015/405036.

El-Sayed Eid M. Polyethylenimine-functionalized magnetic amorphous carbon fabricated from oil palm leaves as a novel adsorbent for Hg(II) from aqueous solutions. Egypt J Pet. 2018;27:1051–60. https://doi.org/10.1016/j.ejpe.2018.03.007.

Folch-Cano C, Yazdani-Pedram M, Olea-Azar C. Inclusion and functionalization of polymers with cyclodextrins: current applications and future prospects. Molecules. 2014;19:14066–79. https://doi.org/10.3390/molecules190914066.

Gao Y, Li G, Zhou Z, Guo L, Liu X. Supramolecular assembly of poly(β-cyclodextrin) block copolymer and benzimidazole-poly(ε-caprolactone) based on host-guest recognition for drug delivery. Colloids Surfaces B Biointerfaces. 2017;160:364–71. https://doi.org/10.1016/j.colsurfb.2017.09.047.

Girish CR, Murty VR. Mass transfer studies on adsorption of phenol from wastewater using lantana camara, forest waste. Int J Chem Eng. 2016;2016:1–11. https://doi.org/10.1155/2016/5809505.

Girish CR, Ramachandra Murty V. Adsorption of phenol from aqueous solution using lantana camara, forest waste: kinetics, isotherm, and thermodynamic studies. Int Sch Res Not. 2014;2014:1–16. https://doi.org/10.1155/2014/201626.

Gopal K, Mohd NI, Raoov M, Suah FBM, Yahaya N, Zain NNM. Development of a new efficient and economical magnetic sorbent silicone surfactant-based activated carbon for the removal of chloro-and nitro-group phenolic compounds from contaminated water samples. RSC Adv. 2019;9:36915–30. https://doi.org/10.1039/c9ra07151b.

Gundogdu A, Duran C, Senturk HB, Soylak M, Ozdes D, Serencam H, Imamoglu M. Adsorption of phenol from aqueous solution on a low-cost activated carbon produced from tea industry waste: equilibrium, kinetic, and thermodynamic study. J Chem Eng Data. 2012;57:2733–43. https://doi.org/10.1021/je300597u.

Guo Y, Liang X, Wang Y, Liu Y, Zhu G, Gui W. Cyclodextrin-based molecularly imprinted polymers for the efficient recognition of pyrethroids in aqueous media. J Appl Polym Sci. 2013;128:4014–22. https://doi.org/10.1002/app.38440.

Hairuddin MN, Mubarak NM, Khalid M, Abdullah EC, Walvekar R, Karri RR. Magnetic palm kernel biochar potential route for phenol removal from wastewater. Environ Sci Pollut Res. 2019;26:35183–97. https://doi.org/10.1007/s11356-019-06524-w.

Han J, Xie K, Du Z, Zou W, Zhang C. β-Cyclodextrin functionalized polystyrene porous monoliths for separating phenol from wastewater. Carbohydr Polym. 2015;120:85–91. https://doi.org/10.1016/j.carbpol.2014.12.011.

Iftekhar S, Ramasamy DL, Srivastava V, Asif MB, Sillanpää M. Understanding the factors affecting the adsorption of Lanthanum using different adsorbents: a critical review. Chemosphere. 2018;204:413–30. https://doi.org/10.1016/j.chemosphere.2018.04.053.

Ismail MGBH, Weng CN, Rahman HA, Zakaria NA. Freundlich isotherm equilibrium equastions in determining effectiveness a low cost absorbent to heavy metal removal in wastewater (Leachate) At Teluk Kitang Landfill, Pengkalan Chepa, Kelantan, Malaysia. J Geogr Earth Sci. 2013;1:01–8.

Ismail NA, Bakhshaei S, Kamboh MA, Abdul Manan NS, Mohamad S, Yilmaz M. Adsorption of phenols from contaminated water through titania-silica mixed imidazolium based ionic liquid: equilibrium, kinetic and thermodynamic modeling studies. J Macromol Sci Part A Pure Appl Chem. 2016;53:619–28. https://doi.org/10.1080/10601325.2016.1212309.

Jain M, Yadav M, Kohout T, Lahtinen M, Garg VK, Sillanpää M. Development of iron oxide/activated carbon nanoparticle composite for the removal of Cr(VI), Cu(II) and Cd(II) ions from aqueous solution. Water Resour Ind. 2018;20:54–74. https://doi.org/10.1016/j.wri.2018.10.001.

Li N, Mei Z, Wei X. Study on sorption of chlorophenols from aqueous solutions by an insoluble copolymer containing β-cyclodextrin and polyamidoamine units. Chem Eng J. 2012;192:138–45. https://doi.org/10.1016/j.cej.2012.03.076.

Lin Q, Wu Y, Jiang X, Lin F, Liu X, Lu B. Removal of bisphenol A from aqueous solution via host-guest interactions based on beta-cyclodextrin grafted cellulose bead. Int J Biol Macromol. 2019;140:1–9. https://doi.org/10.1016/j.ijbiomac.2019.08.116.

Liu F, Chen C, Qian J. Film-like bacterial cellulose/cyclodextrin oligomer composites with controllable structure for the removal of various persistent organic pollutants from water. J Hazard Mater. 2021;405:124122. https://doi.org/10.1016/j.jhazmat.2020.124122.

Magdy YM, Altaher H, ElQada E. Removal of three nitrophenols from aqueous solutions by adsorption onto char ash: equilibrium and kinetic modeling. Appl Water Sci. 2018;8:1–15. https://doi.org/10.1007/s13201-018-0666-1.

Mahmad MKN, Baharun N, Remy Rozainy MAZM, Ismail S, Putra TAR, Abdul Wahab SARS. Adsorption isotherm study in the removal of As (V) by Schwertmannite. In: AIP Conf Proc, vol. 2030. 2018. https://doi.org/10.1063/1.5066832.

Mohamed EF, Andriantsiferana C, Wilhelm AM, Delmas H. Competitive adsorption of phenolic compounds from aqueous solution using sludge-based activated carbon. Environ Technol. 2011;32:1325–36. https://doi.org/10.1080/09593330.2010.536783.

Mohammadzadeh Kakhki R. Application of magnetic nanoparticles modified with cyclodextrins as efficient adsorbents in separation systems. J Incl Phenom Macrocycl Chem. 2015;82:301–10. https://doi.org/10.1007/s10847-015-0512-0.

Monteiro APF, Caminhas LD, Ardisson JD, Paniago R, Cortés ME, Sinisterra RD. Magnetic nanoparticles coated with cyclodextrins and citrate for irinotecan delivery. Carbohydr Polym. 2017;163:1–9. https://doi.org/10.1016/j.carbpol.2016.11.091.

Moulahcene L, Kebiche-Senhadji O, Skiba M, Lahiani-Skiba M, Oughlis-Hammache F, Benamor M. Cyclodextrin polymers for ibuprofen extraction in aqueous solution: recovery, separation, and characterization. Desalination Water Treat. 2016;57:11392–402. https://doi.org/10.1080/19443994.2015.1048734.

Ozdes D, Duran C, Senturk HB, Avan H, Bicer B. Kinetics, thermodynamics, and equilibrium evaluation of adsorptive removal of methylene blue onto natural illitic clay mineral. Desalination Water Treat. 2014;52:208–18. https://doi.org/10.1080/19443994.2013.787554.

Paquin F, Rivnay J, Salleo A, Stingelin N, Silva-Acuña C. Multi-phase microstructures drive exciton dissociation in neat semicrystalline polymeric semiconductors. J Mater Chem c. 2015;3:10715–22. https://doi.org/10.1039/c5tc02043c.

Phatthanakittiphong T, Seo GT. Characteristic evaluation of graphene oxide for bisphenol a adsorption in aqueous solution. Nanomaterials. 2016;6:128. https://doi.org/10.3390/nano6070128.

Raoov M, Mohamad S, Abas MR. Removal of 2,4-dichlorophenol using cyclodextrin-ionic liquid polymer as a macroporous material: characterization, adsorption isotherm, kinetic study, thermodynamics. J Hazard Mater. 2013;263:501–16. https://doi.org/10.1016/j.jhazmat.2013.10.003.

Rashid S, Mazlan NA, Sapari JM, Raoov Ramachandran M, Pandian Sambasevam K. Fabrication of magnetic nanoparticles coated with polyaniline for removal of 2, 4-dinitrophenol. J Phys Conf Ser. 2018;1123:012015. https://doi.org/10.1088/1742-6596/1123/1/012015.

Santhosh C, Nivetha R, Kollu P, Srivastava V, Sillanpää M, Grace AN, Bhatnagar A. Removal of cationic and anionic heavy metals from water by 1D and 2D-carbon structures decorated with magnetic nanoparticles. Sci Rep. 2017;7:1–11. https://doi.org/10.1038/s41598-017-14461-2.

Sas OG, Castro M, Domínguez Á, González B. Removing phenolic pollutants using deep eutectic solvents. Sep Purif Technol. 2019;227:115703. https://doi.org/10.1016/j.seppur.2019.115703.

Sas OG, Sánchez PB, González B, Domínguez Á. Removal of phenolic pollutants from wastewater streams using ionic liquids. Sep Purif Technol. 2020;236:116310. https://doi.org/10.1016/j.seppur.2019.116310.

Shahriman MS, Mohamad Zain NN, Mohamad S, Abdul Manan NS, Yaman SM, Asman S, Raoov M. Polyaniline modified magnetic nanoparticles coated with dicationic ionic liquid for effective removal of rhodamine B (RB) from aqueous solution. RSC Adv. 2018;8:33180–92. https://doi.org/10.1039/C8RA06687F.

Spiridon OB, Dascălu D, Mateescu M, Nartiță R. Comparative study concerning the removal of phenol from wastewater on sludge and zeolite. New Front Chem. 2015;24:109–20.

Surikumaran H, Mohamad S, Sarih NM. Molecular imprinted polymer of methacrylic acid functionalized β-Cyclodextrin for selective removal of 2,4-dichlorophenol. Int J Mol Sci. 2014;15:6111–36. https://doi.org/10.3390/ijms15046111.

Surikumaran H, Mohamad S, Muhamad Sarih N, Raoov M. β-cyclodextrin based molecularly imprinted solid phase extraction for class selective extraction of priority phenols in water samples. Sep Sci Technol. 2015;50:2342–51. https://doi.org/10.1080/01496395.2015.1043016.

Tahermansouri H, Dehghan Z, Kiani F. Phenol adsorption from aqueous solutions by functionalized multiwalled carbon nanotubes with a pyrazoline derivative in the presence of ultrasound. RSC Adv. 2015;5:44263–73. https://doi.org/10.1039/c5ra02800k.

Theydan SK, Ahmed MJ. Adsorption of methylene blue onto biomass-based activated carbon by FeCl3 activation: equilibrium, kinetics, and thermodynamic studies. J Anal Appl Pyrolysis. 2012;97:116–22. https://doi.org/10.1016/j.jaap.2012.05.008.

Tursi A, Chatzisymeon E, Chidichimo F, Beneduci A, Chidichimo G. Removal of endocrine disrupting chemicals from water: adsorption of bisphenol-a by biobased hydrophobic functionalized cellulose. Int J Environ Res Public Health. 2018;15:2419–31. https://doi.org/10.3390/ijerph15112419.

Wang Z, Ge H, Wang X, Ye C, Fan S. Mono and co-immobilization of imidazolium ionic liquids on silica: Effects of the substituted groups on the adsorption behavior of 2,4-dinitrophenol. RSC Adv. 2019;9:32425–34. https://doi.org/10.1039/c9ra07635b.

Wardani RK, Dahlan K, Wahyudi ST, Sukaryo SG. Synthesis and characterization of nanoparticle magnetite for biomedical application. Int J Biol Macromol. 2019;2194:020137–42. https://doi.org/10.1016/j.ijbioma10.1063/1.5139869c.2020.02.313.

Wu GQ, Sun XY, Hui H, Zhang X, Yan J, Zhang QS. Adsorption of 2,4-dichlorophenol from aqueous solution by activated carbon derived from moso bamboo processing waste. Desalination Water Treat. 2013;51:4603–12. https://doi.org/10.1080/19443994.2012.751053.

Xiao G, Fu L, Li A. Enhanced adsorption of bisphenol A from water by acetylaniline modified hyper-cross-linked polymeric adsorbent: effect of the cross-linked bridge. Chem Eng J. 2012;191:171–6. https://doi.org/10.1016/j.cej.2012.02.092.

Yang M, Huang Y, Yue Q, Cao H, Li X, Lin Y. Preparation of a novel polymeric adsorbent and its adsorption of phenol in aqueous solution. Desalination Water Treat. 2016;57:13295–306. https://doi.org/10.1080/19443994.2015.1055814.

Zain NNM, Abu Bakar NK, Mohamad S. Study of removal of phenol species by adsorption on non-ionic silicon surfactant after cloud point extraction methodology. Desalination Water Treat. 2016;57:3532–43. https://doi.org/10.1080/19443994.2014.987176.

Zhou X, Lai C, Huang D, Zeng G, Chen L, Qin L, Xu P, Cheng M, Huang C, Zhang C, Zhou C. Preparation of water-compatible molecularly imprinted thiol-functionalized activated titanium dioxide: Selective adsorption and efficient photodegradation of 2, 4-dinitrophenol in aqueous solution. J Hazard Mater. 2018;346:113–23. https://doi.org/10.1016/j.jhazmat.2017.12.032.

Publisher's Note